AMERICAN SOCIETY FOR MICROBIOLOGY | mBio®

RESEARCH ARTICLE

Using *Entamoeba muris* To Model Fecal-Oral Transmission of *Entamoeba* in Mice

Carolina Mendoza Cavazos,[a,b] Marienela Y. Heredia,[b,c] Leah A. Owens,[d] Laura J. Knoll[b]

[a]Microbiology Doctoral Training Program, University of Wisconsin-Madison, Madison, Wisconsin, USA
[b]Department of Medical Microbiology and Immunology, University of Wisconsin-Madison, Madison, Wisconsin, USA
[c]Cellular and Molecular Pathology Graduate Program, University of Wisconsin-Madison, Madison, Wisconsin, USA
[d]Department of Pathobiological Sciences, University of Wisconsin-Madison, School of Veterinary Medicine, Madison, Wisconsin, USA

ABSTRACT There are several *Entamoeba* species that colonize humans, but only *Entamoeba histolytica* causes severe disease. *E. histolytica* is transmitted through the fecal-oral route to colonize the intestinal tract of 50 million people worldwide. The current mouse model to study *E. histolytica* intestinal infection directly delivers the parasite into the surgically exposed cecum, which circumvents the natural route of infection. To develop a fecal-oral mouse model, we screened our vivarium for a natural murine *Entamoeba* colonizer via a pan-*Entamoeba* PCR targeting the 18S ribosomal gene. We determined that C57BL/6 mice were chronically colonized by *Entamoeba muris*. This amoeba is closely related to *E. histolytica*, as determined by 18S sequencing and cross-reactivity with an *E. histolytica*-specific antibody. In contrast, outbred Swiss Webster (SW) mice were not chronically colonized by *E. muris*. We orally challenged SW mice with 1×10^5 *E. muris* cysts and discovered they were susceptible to infection, with peak cyst shedding occurring between 5 and 7 days postinfection. Most infected SW mice did not lose weight significantly but trended toward decreased weight gain throughout the experiment compared to mock-infected controls. Infected mice treated with paromomycin, an antibiotic used against noninvasive intestinal disease, do not become colonized by *E. muris*. Within the intestinal tract, *E. muris* localizes exclusively to the cecum and colon. Purified *E. muris* cysts treated with bovine bile *in vitro* excyst into mobile, pretrophozoite stages. Overall, this work describes a novel fecal-oral mouse model for the important global pathogen *E. histolytica*.

IMPORTANCE Infection with parasites from the *Entamoeba* genus are significantly underreported causes of diarrheal disease that disproportionally impact tropical regions. There are several species of *Entamoeba* that infect humans to cause a range of symptoms from asymptomatic colonization of the intestinal tract to invasive disease with dissemination. All *Entamoeba* species are spread via the fecal-oral route in contaminated food and water. Studying the life cycle of *Entamoeba*, from host colonization to infectious fecal cyst production, can provide targets for vaccine and drug development. Because there is not an oral challenge rodent model, we screened for a mouse *Entamoeba* species and identified *Entamoeba muris* as a natural colonizer. We determine the peak of infection after an oral challenge, the efficacy of paromomycin treatment, the intestinal tract localization, and the cues that trigger excystation. This oral infection mouse model will be valuable for the development of novel therapeutic options for *Entamoeba* infections.

KEYWORDS *Entamoeba*, parasitology, fecal-oral, intestinal infection, excystation

Parasitic diseases are underappreciated causes of morbidity and mortality because disease outcomes are variable (1), cases are often underreported (2), and disease disproportionately impacts geographical locations experiencing poverty (1–3). Diarrheal diseases

Editor Patricia J. Johnson, University of California Los Angeles

Address correspondence to Laura J. Knoll, ljknoll@wisc.edu.

The authors declare no conflict of interest.

Received 26 October 2022
Accepted 9 January 2023
Published 6 February 2023

are a significant and underreported cause of child mortality in tropical regions (4, 5). Such infections are exacerbated by factors such as resource availability, lack of sanitation infrastructure, and malnutrition (6). For these reasons, diarrheal diseases represent a long-standing and significant burden, particularly in Latin America, Southeast Asia, and sub-Saharan Africa (6). Diarrheal diseases are caused by a range of pathogens, such as bacteria, viruses, and parasites, including *Entamoeba histolytica*. *E. histolytica* is an extracellular parasite that causes human infection with variable outcomes ranging from asymptomatic colonization to diarrhea, invasive colitis, liver abscesses, and metastatic infection. *E. histolytica* ranks among the top 15 causes of diarrhea in children under the age of 2 in developing countries (7, 8). Prevalence rates vary significantly due to earlier misdiagnoses resulting from use of microscopy as a diagnostic tool, which is unable to differentiate between *E. histolytica* and the nonpathogenic *Entamoeba dispar*.

Entamoeba infection starts with the ingestion of the cyst stage from contaminated food or water. Presumably in the small intestine, the *Entamoeba* cyst molts from its chitinous shell and differentiates into the metabolically active trophozoite form through a process known as excystation. Trophozoites then attach to the intestinal epithelium where they undergo asexual reproduction and encystation. The infectious fecal cysts are shed and contaminate the environment to complete the parasite life cycle. Trophozoites can either stay contained within the intestinal tract or may disseminate to soft tissue organs like the liver, the lungs, or the brain (9–12), although in ~90% of the cases, the infection remains in the intestinal lumen (13, 14). The current murine intestinal infection model surgically delivers trophozoites into the cecum of animals and has provided immense insight into host-pathogen interactions but produces no cysts (15). To date, attempts at generating cysts *in vitro* using the *E. histolytica* reference strain, HM1:IMSS, have successfully yielded cyst-like structures (CLS) resembling immature cysts (16–18). However, the infectivity of these CLS in an animal infection model has not yet been determined, and efficient production of mature cysts has not yet been achieved. Thus, modeling the critical developmental stage interconversion that *E. histolytica* undergoes between ingestion and colonization of the cecum is not yet possible (19). A model that includes the developmental changes of excystation and encystation would allow the field to understand the transmission of the pathogen and find targets for intervention (reviewed in reference 20), as only viable parasites completely encysted and shed via the fecal-oral route can contaminate food and water and infect a new host.

The parasitology field has used species that naturally colonize animals to expand the knowledge of infectious diseases that are fastidious to culture or model in the laboratory. Murine pathogens like *Plasmodium chabaudi* have been pivotal to studying the *in vivo* pathology of malaria. For the *Entamoeba* field, *Entamoeba invadens*, a reptile-specific pathogen, has provided critical insights related to developmental changes like encystation. Here, we screened for a natural murine *Entamoeba* colonizer and developed an oral infection model using Swiss Webster (SW) mice. SW mice treated with paromomycin showed no *E. muris* colonization. We further determine infection location within the intestinal tract and excystation cues for the purified fecal cysts.

RESULTS

C57BL/6 mice, but not Swiss Webster mice, are chronically colonized with a naturally occurring *Entamoeba* organism. We screened transgenic and wild-type animals within our vivarium facility (Fig. 1A) using a Pan-*Entamoeba* PCR (Fig. S1). We screened fecal material from males and females with ages ranging from newly weaned to mice that spent up to a 1 year in our facility. Eighty percentage of the mice from the C57BL/6 background were colonized with an *Entamoeba* organism. To address if an *Entamoeba* is naturally occurring in other vivariums, we requested fecal samples from C57BL/6 mice from five collaborators around the country ($n = 18$) and ran both single-step pan-*Entamoeba* PCR and 2-step, nested PCR on all samples obtained. We were able to detect *Entamoeba* gDNA using single-step PCR in samples from one other institution, while for another institution, we were only able to detect the parasite using nested PCR (Table S1). Colonization was by no means ubiquitous, as the majority of

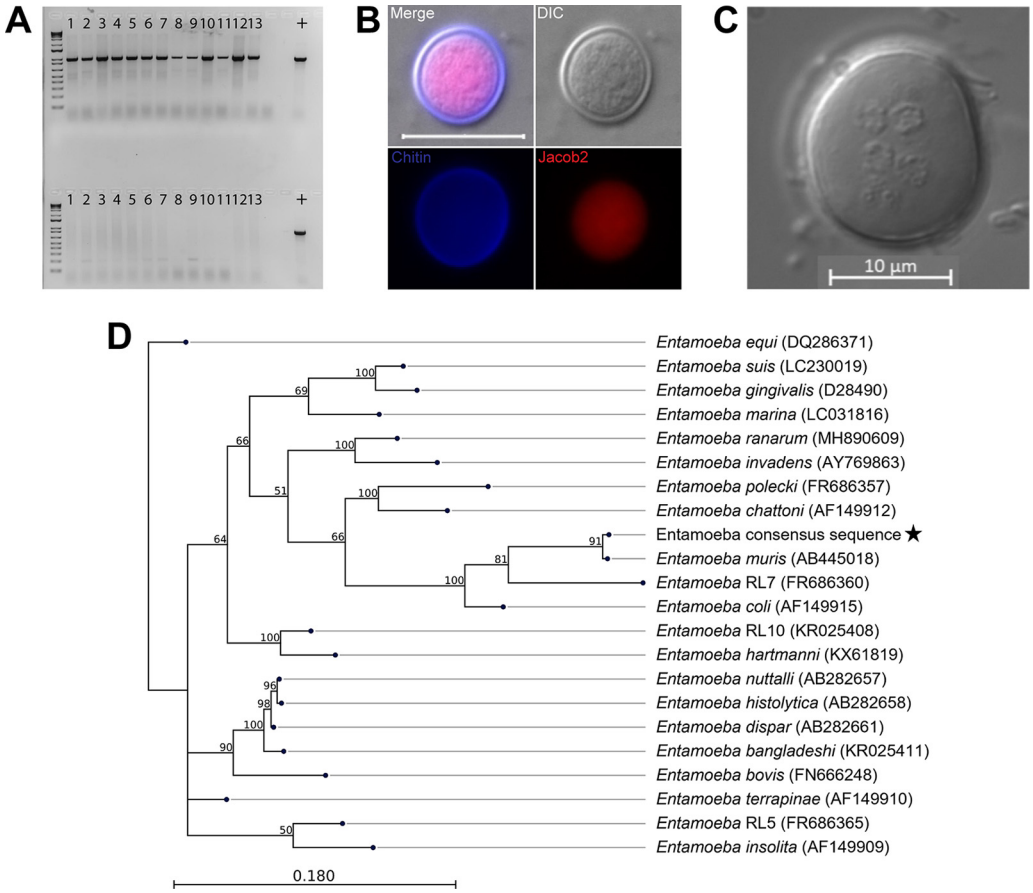

FIG 1 Identification of a murine Entamoeba species. (A) Representative Pan-Entamoeba PCR for C57BL/6 mice (top) and Swiss Webster mice (bottom) within our vivarium. The loading control was murine GAPDH (data not shown). Each lane number represents a mouse cage. Positive control (+) is isolated genomic DNA from axenic *Entamoeba histolytica* culture. (B) Immunofluorescence assay staining for chitin (Calcofluor White), Jacob2 (1A4 antibody), scale bar represents 20 μm. (C) Representative phenotypic characterization of the number of nuclei of E. muris cysts (>4 nuclei). Image was taken using DIC. Scale bar represents 10 μm. (D) 18S phylogeny is based on a 1,033 bp alignment, including 27 published Entamoeba sequences, labeled as species name (NCBI accession), plus the Entamoeba found in our vivarium, indicated by a star. Numbers on branches are bootstrap values (%) based on 1,000 replicates (values >50% are shown). The scale bar indicates nucleotide substitutions per site.

these institutions were PCR-negative even after using the nested PCR approach (Table S1). In contrast, all the SW mice from our vivarium tested were PCR negative, regardless of age or sex (Fig. 1A).

To confirm the PCR findings in our animals, we developed a sucrose density gradient protocol based on fecal isolation methods from the *Entamoeba* literature (21) (Fig. S2) and conducted phenotypic characterization of the isolated cysts (Fig. 1B and C). We processed feces of PCR-positive mice within a sucrose gradient of 1.33 specific gravity and isolated structures of 15 to 20 μm in diameter. These structures were cyst-like and stained with Calcofluor White, indicating the presence of chitin (Fig. 1B). We further characterized these cysts by immunofluorescence detection of a previously published *Entamoeba*-specific antibody targeting the lectin Jacob2 (22). The sucrose gradient results for B6 and SW mice were 100% replicative of the Pan-*Entamoeba* PCR; SW mice did not display cyst-like structures in their fecal samples, while the B6 fecal samples contained 15 to 20 μm-diameter cysts that stained positive for both chitin and Jacob2 (Fig. 1B). We also observed the presence of multiple nuclei within individual cysts (Fig. 1C).

To determine the species of *Entamoeba* present in our mice, we gel-purified and Sanger-sequenced the 1 kb pan-*Entamoeba* PCR product from cecum, colon, and fecal samples from 8 mice (n = 24 total). The resulting reads were 100% identical to each

other and most closely matched *Entamoeba muris* (GenBank accession number AB445018) with 98% query coverage at 92% identity and an E value of 0.00. We then performed phylogenetic analysis to further confirm this preliminary species identification. Alignment of 21 published *Entamoeba* 18S sequences from NCBI GenBank along with our consensus Sanger sequence yielded a final alignment length of 1,033 bp. A maximum-likelihood phylogeny built from this alignment shows our organism to cluster with *Entamoeba muris*, as expected from the BLASTn results, and form a clade with *Entamoeba* RL7 and *Entamoeba coli* (Fig. 1D). Pairwise comparison of the *E. muris/coli* clade based on the 18S phylogenetic tree across the entire length of the alignment shows our organism to be 91.63% identical to *E. muris* with 9 total alignment gaps (0.87%) compared to 81.82% identity and 42 gaps (4.1%) with its next-closest relative, *Entamoeba* RL7 (Table S2). Thus, we will refer to this organism as *E. muris* here.

Swiss Webster mice are susceptible to *Entamoeba muris* oral challenge. As SW mice were not currently colonized, we determined if these mice were suitable for *E. muris* infection and characterization using an oral challenge model. When orally challenged with a low cyst dosage (1×10^5 isolated from B6 mice), SW mice were able to host a patent infection, as evidenced by fecal cyst shedding, but displayed asymptomatic infections in all cases. Specifically, we did not observe any hallmark signs or symptoms of distress among our infected SW mice during our daily health checks. We also did not see any notable changes in grooming, movement, food and water consumption, or overall activity that would indicate symptomatic disease caused by *E. muris*. We tracked changes in host weight during the infection and found that both uninfected and infected animals displayed a modest degree of variability in weight changes, with most mice gaining weight over time (Fig. 2A and S3A). No statistically significant differences in weight change were found between uninfected animals and animals orally challenged with *E. muris* cysts. Despite this, infected mice seemed to display an overall trend in slower weight gain compared to uninfected control mice (Fig. 2A). Weight loss was only observed for one of the biological replicates (Fig. S3A) and was not correlated with cyst shedding (Fig. S3B). Fecal samples showed cysts as early as 3 days postinfection (dpi) via sucrose gradient. When using this method, we determined the peak of infection to be 7 dpi based on average cysts counts across four independent infection replicates ($n = 27$ mice, 17 infected and 10 uninfected controls). Shedding per biological replicates does not show significant differences (Fig. S3B). By sucrose gradient, we detected a significant decrease in cyst shedding by 11 dpi, and very few *E. muris* cysts were detected using this method by 28 dpi, indicating a sharp decline in viable cyst shedding.

Using a similar approach to the Pan-*Entamoeba* screen, we designed qPCR detection primers that amplified a 200-bp amplicon to quantify *E. muris* shedding. We generated a standard curve using cyst samples of known concentrations based on counts, ranging from 1,562 cysts to 100,000 cysts on a 2-fold scale (Fig. S4A). Our qPCR results determined that *E. muris* was detectable as early as 3 dpi, in accordance with the sucrose gradient isolation. However, the peak of infection was at 5 dpi, and a significant reduction was evident by 9 dpi. In contrast to our sucrose gradient data (Fig. 2B), SW mice appear to maintain infection by *E. muris* up to 28 dpi when using qPCR as a detection method. Taken together, these results suggest that qPCR detection occurs prior to peak viable cyst isolation and that SW mice may remain colonized by *E. muris* even after viable cysts are no longer being shed.

Paromomycin treatment prevents colonization of *Entamoeba muris*. Patients infected with *E. histolytica* are prescribed antibiotics depending on the degree of pathogenicity. Two common drug treatments for patients infected with *E. histolytica* are metronidazole and paromomycin. For invasive disease, metronidazole is the gold standard for treatment, but some *E. histolytica* strains can develop resistance over time (23). Paromomycin is the treatment of choice for noninvasive *E. histolytica* infections (24) due to its antimicrobial activity against facultative anaerobes and lack of absorption in the gut. To determine if paromomycin recapitulates its amoebicidal effect against *E. muris*, we orally infected SW mice with 7×10^4 cysts isolated from B6 mice and immediately began treatment with paromomycin (16 g/L) in their

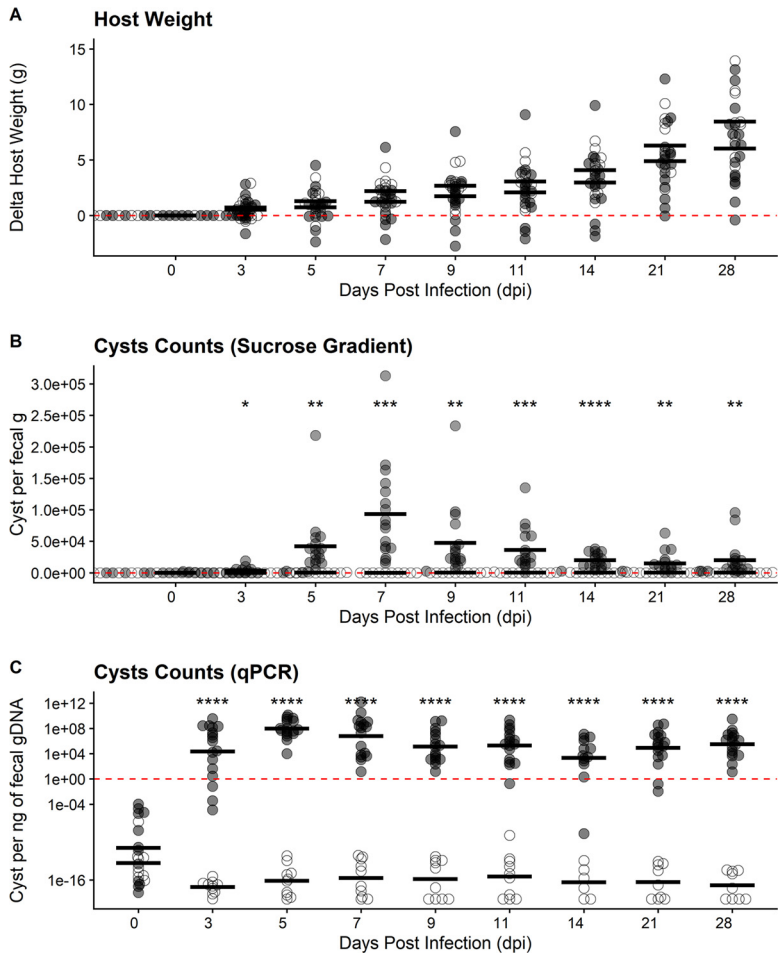

FIG 2 Swiss Webster mice are susceptible to *Entamoeba muris* oral challenge. (A) Host weight was monitored through the course of infection. (B) Quantification of cysts isolated by sucrose gradient from Swiss Webster fecal samples (normalized by fecal mass). Peak of infection was determined to be 7 dpi. (C) Quantification of cysts in fecal samples via qPCR isolated from Swiss Webster's fecal samples (normalized by gDNA per qPCR). Each dot represents a single mouse (n = 27 mice, 17 infected and 10 uninfected controls). Open circles represent uninfected mice while gray circles represent infected mice. Significance was determined using a two-tailed t test between the uninfected versus infected average per DPI. Data combines four independent biological replicates (see Fig. S3 for individual biological replicate [n = 4] plotting).

drinking water for the first 7 days postinfection before reverting to untreated drinking water. Using the approaches presented earlier, we monitored *E. muris* colonization and host weight for 2 weeks postinfection. Overall, SW mice treated with paromomycin showed higher variability in weight changes throughout the course of treatment compared to untreated mice (Fig. S5). Infected mice treated with paromomycin again trended toward slower weight gain than their uninfected treated counterparts, although this observation was not statistically significant (Fig. S5). In contrast, both uninfected and infected mice given untreated drinking water displayed similar weight changes over the course of 14 days (Fig. S5). As expected, SW mice that were challenged with *E. muris* but received no paromomycin treatment shed fecal cysts as early as 3 to 5 dpi via sucrose gradient (Fig. 3A), even at a lower infectious dose of 7×10^4 cysts. In concordance with our previous results, cyst shedding peaked at 7 dpi and declined significantly by 9 dpi (Fig. 3A). In contrast, SW mice challenged with *E. muris* and treated with paromomycin never shed any viable *E. muris* throughout 14 dpi as determined by sucrose gradient isolation (Fig. 3A).

We also monitored *E. muris* shedding via qPCR as a second method of detection. In agreement with our sucrose gradient data (Fig. 3A), the peak of infection in untreated mice challenged with *E. muris* was also found to be 7 dpi by qPCR (Fig. 3B). Unlike our

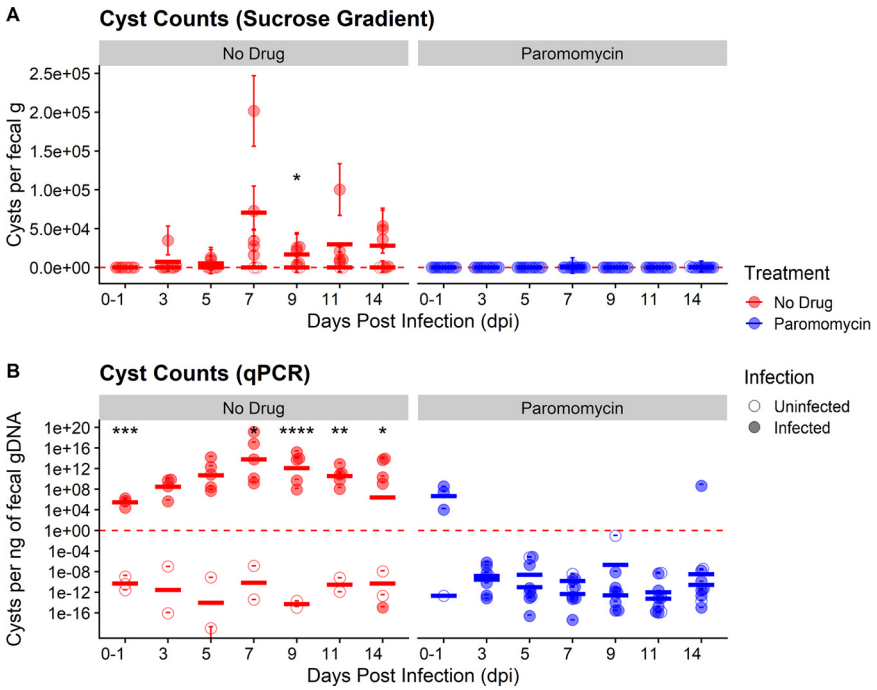

FIG 3 Paromomycin effectively inhibits colonization of SW mice by *Entamoeba muris*. (A) Quantification of cysts isolated by sucrose gradient from (Swiss Webster fecal samples normalized by fecal mass). (B) Quantification of cysts in fecal samples via qPCR isolated from Swiss Webster fecal samples (normalized by gDNA per qPCR). Each circle represents a single mouse (n = 16 mice, 12 infected and 4 uninfected controls). Open circles represent uninfected mice while filled circles represent infected mice. Red circles represent untreated mice while blue circles represent mice treated with paromomycin. Bars indicate calculated mean values for each experimental group per DPI. Significance was determined using a two-tailed t test between the uninfected versus infected average per DPI. Data combines two independent biological replicates.

sucrose gradient data, qPCR results indicated that all infected mice did have detectable *E. muris* between the day of infection (0 dpi) to 1 dpi (Fig. 3B). However, infected mice treated with paromomycin no longer shed detectable *E. muris* by 3 dpi (Fig. 3B). These mice continued to lack detectable *E. muris* up to 14 dpi, except for one mouse on day 14 (Fig. 3B). Taken together, these results suggest that paromomycin effectively inhibits *E. muris* colonization when administered as a prophylactic and that our model can be used for drug screening studies relevant to luminal *Entamoeba* infections.

***Entamoeba muris* resides in the large intestine at 5 days postinfection.** *E. histolytica* is thought to replicate in the colon and has been found during diagnostic colonoscopies (25). As our model uses the natural oral route of infection, we aimed to determine where *E. muris* is located during primary infection. We infected SW mice with 10^5 cysts by oral gavage and collected the intestinal content and mucus layer of murine gastrointestinal sections at 5 dpi, when most of the animals were shedding cysts by qPCR detection (Fig. 2C). The small intestine was sectioned into three parts: duodenum (D), jejunum (J), and ileum (I). The cecum (Ce) and the colon (Co) correspond to the large intestine (Fig. 4A). As a positive control for the presence of cysts, we included two fresh fecal pellets (F) and we used a standard loading control, murine GAPDH (Fig. 4B, lower panel). As expected from clinical data (reviewed in reference 26), *Entamoeba* localizes within the large intestine (Fig. 4B, upper panel). While we found mouse to mouse variability between levels of *E. muris* detection within the cecum, colon, and fecal samples, no *Entamoeba muris* gDNA was isolated from the small intestine (Fig. 4B, upper panel).

Bile extract triggers *Entamoeba muris* excystation *in vitro*. To determine if the previously published *E. invadens* cues could trigger consistent *E. muris* excystation *in vitro*, we incubated the isolated cysts with Nanopure water, 80 mM sodium bicarbonate, 1% bovine bile, or a combination of both treatments for 24 h (27). We scored excystation efficiency based on the percentage of the parasite that was outside the chitin shell. An intact cyst was given a score of 0 (Fig. 1B). We scored an open cyst with less than 50% of the trophozoite-

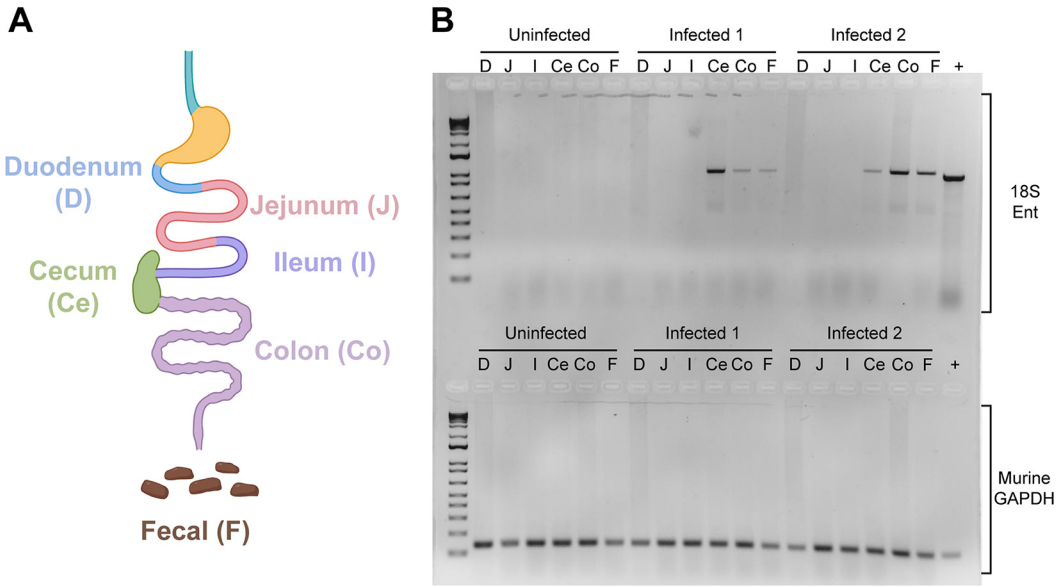

FIG 4 *Entamoeba muris* localizes to the large intestine of infected animals. (A) Schematics of the murine intestine. (B) The *Entamoeba* 18S gene was amplified from gastrointestinal sections (gel top). The positive control is genomic DNA extracted from an *Entamoeba histolytica* axenic culture. As a loading control, the murine GAPDH gene was amplified from various gastrointestinal sections, with gDNA isolated from mice tail snips serving as a positive control (gel bottom). Gel image is a representative of two independent biological replicates (n = 6, 4 infected and 2 uninfected controls).

mass excysted as a 1, cysts where 50% or more of the parasite was outside the chitin shell as a 2, and empty chitin shells were given a score of 3 (Fig. 5A). We observed excystation to be an asynchronous process, as scores ranged within each condition (Fig. S6). Treatment of cysts with only 1% bovine bile resulted in greater than 70% excystation by 24 h, which was statistically higher than the excystation rate of the Nanopure water treatment (P = 0.0040). This excystation rate was not enhanced by the addition of the sodium bicarbonate, and sodium bicarbonate alone did not significantly enhance excystation compared to water only (Fig. 5B). These results strongly indicate that 1% bile is sufficient to trigger excystation, which implies that excystation of *E. muris* is occurring in the small intestinal tract as we would expect.

DISCUSSION

To the best of our knowledge, this work is the first to demonstrate that C57BL/6 mice can be chronically colonized with *E. muris*. C57BL/6 mice have been previously

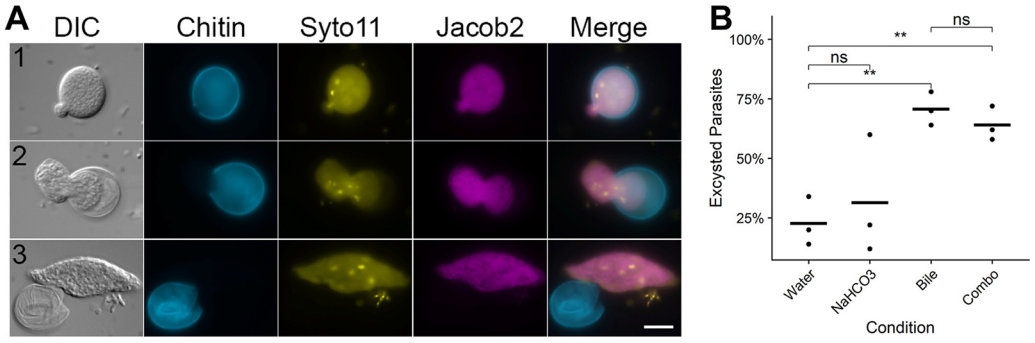

FIG 5 *Entamoeba muris* shows reliable excystation *in vitro* when treated with upper gastrointestinal tract components. Fecal cysts were purified by sucrose density gradient and then acid washed (0.1 M HCl). Cysts were inoculated into excystation conditions (1% bovine bile, 80 mM sodium bicarbonate, or a combination of both), then incubated for 24 h at room temperature. (A) Cysts were scored from 0 to 3, where 0 represented an intact cyst and 3 is an empty chitin shell. Chitin (Calcofluor White), Jacob2 (1A4 antibody [17]), and nuclei (Syto11). Scale bar represents 10 μm. (B) Excystation rates (score $\geq$ 1) were quantified under these conditions. Significance was determined using a two-tailed t test. Only significant pairwise comparisons are shown; Bile (P = 0.004) and, $NaHCO_3$ + Bile (P = 0.0064). Each dot represents a biological replicate (n = 3 independent experiments), black horizontal line is the average of the three biological replicates.

described as naturally resistant to *E. histolytica* when injecting trophozoites directly into a surgically exposed cecum (28). Other protozoans, such as *Tritrichomonas musculis*, have been reported to chronically colonize many mouse colonies on the East Coast of the United States (29). *T. musculis* was found to change the immune response to protect against pathogens in mice with chronic colonization, and *E. muris* may also be changing the immune responses. Understudied intestinal protozoans may account for the variability of results between research institutions. Many of the fecal samples from C57BL/6 mice across the United States did not amplify *Entamoeba*, but the gDNA isolated from the feces was of high quality because we could detect host gDNA in the *Entamoeba* negative samples when using a primer set for murine GAPDH. One of the limitations of this study is that the *Entamoeba* identification is based on the 18S gene (Fig. 1D and Table S2) and phenotypic characterization of the number of nuclei (>4) via microscopy (Fig. 1C); thus, further characterization will be required.

One surprising result was the positive Jacob2 staining for the *E. muris* cysts (Fig. 1B) given the genetic divergence we observed in our phylogenetic analyses of the *E. muris* 18S ribosomal gene (Fig. 1D). The 1A4 antibody was previously described to distinguish *E. histolytica* cysts without cross-reacting either with *E. dispar* or *E. bangladeshi* cysts. The 1A4 antibody was generated against the flexible, serine-rich spacer of the Jacob2 lectin in *E. histolytica* (22), so perhaps this region is similar in *E. muris*. It is also interesting that the *E. muris* cyst Jacob2 staining is associated with the pretrophozoite during excystation and not the chitin-rich wall (Fig. 4), as previously shown in stool samples and xenic cultures with another anti-Jacob2 antibody (30). Thus, *E. muris* may be a good model organism for comparative studies examining *Entamoeba* species convergence and divergence at both the structural and genetic level.

We demonstrated that previously uninfected SW mice can be infected with *E. muris* via oral gavage, sustain replication of *E. muris* in the gut, and shed intact cysts, recapitulating the stage interconversion processes that constitute the *Entamoeba* life cycle. We were especially interested in the natural route of infection as it has been established that the route of infection impacts disease progression for other parasites like *Toxoplasma gondii* (31, 32). Because SW are outbred mice, they have been used for the evaluation of vaccines due to their unbiased immune response (33). In contrast, inbred mice of various genetic backgrounds exhibit different immune responses to an infectious challenge (34), specifically for parasitic infections that are intracellular (35) or extracellular (36). Inbreeding within human populations has been linked to protection against malaria (37), but inbreeding in wild European badgers intensified sex- and age-dependent tuberculosis disease (38). Considering these factors, our *E. muris* oral infection model may be useful for investigations into host variations in susceptibility and transmissibility of *Entamoeba* via use of collaborative cross mice (39). Indeed, future studies will examine *E. muris* oral infection in other inbred and outbred mice as well as immune deletion strains to determine the inflammatory responses necessary for *Entamoeba* control.

We also demonstrate that SW mice can be protected from *E. muris* infection oral infection using paromomycin. A surprising result from these experiments was that mice treated with paromomycin exhibited higher variability in weight changes compared to untreated mice (Fig. S5). This observation may hint at subtle differences in how a host responds to antibiotic treatment. In addition, paromomycin served as an effective prophylactic by inhibiting *E. muris* colonization after oral infection, demonstrated by a complete lack of cyst shedding as quantified by sucrose gradient (Fig. 3A) and no qPCR detection by 3 dpi (Fig. 3B). However, most patients do not take anti-parasitic drugs as prophylaxis, but rather as treatment for an already established infection. In our paromomycin treatment studies, we did observe early detection of *E. muris* in infected mice by qPCR at 1 dpi but not by 3 dpi. This early but transient detection could be attributed to *E. muris* cysts passively shed in the feces as a by-product of oral infection or early colonization of parasites that were later killed by paromomycin treatment. Although more studies are needed to demonstrate that paromomycin can directly kill an active *E. muris* infection in SW mice, these experiments are a proof of principle that our *E. muris* oral infection model can be applied to

characterization of currently available anti-parasitic drugs. While drug development must be particularly targeted against *E. histolytica*, we foresee our *E. muris* oral infection model proving useful for the discovery and testing of novel anti-amebic compounds broadly effective against all *Entamoeba* species, not just *E. histolytica*.

Contrary to our expectations, about 20% of cysts isolated from unfixed fecal material via a sucrose gradient undergo asynchronous excystation when stored overnight at 4°C in Nanopure water. These results are surprising because, for axenic *Entamoeba invadens*, a combination of cues encountered in the upper gastrointestinal tract are required for comparable levels of excystation (27). Perhaps chemical signals present in the fecal samples, not eliminated during the sucrose gradient purification and not present in *E. invadens* literature, are triggering excystation in the isolated cysts. It may also be possible that exposure to sucrose during density gradient purification may serve as a nutritional cue for *E. muris* to excyst at low levels. The experimental induction of excystation with the bile treatment alone was also surprising because for *E. invadens*, bile alone yields less than 40% excystation (27). This may allude to differences between reptilian and murine hosts in gut physiology and metabolism. We did not perform the water pretreatment as described in the *E. invadens* protocol. Perhaps our isolation process (Fig. S2) might act as a water pretreatment, given the excystation yield of treatment with bile alone is comparable to the combination treatment previously reported (27).

There was a significant difference in the number of parasites quantified when using qPCR detection versus sucrose gradient isolation. This result is an important limitation that might be explained by the nature of the two selected assays. The sucrose isolation protocol selects for healthy cysts with a specific gravity of 1.33. A parasite that is in the trophozoite state, currently excysting, or that has a suboptimal cyst wall would be lost during the density gradient protocol. Meanwhile, the qPCR assay detects parasites in any state regardless of viability. In addition, each cyst can contain more than 4 nuclei, further increasing the amount of detectable *E. muris* gDNA in fecal samples.

During this project, we also discovered the importance of humidity on cyst viability, which has been characterized previously in other diarrhea causing parasites (40). Vivarium records indicate that there are drastic differences in humidity between the winter (20%) and summer (50%). The number of cysts isolated that were "healthy" and presumably viable at the specific gravity of 1.33 (Fig. S2B, pellet 3) was dramatically reduced during the winter months. When we examined the waste sections of the gradient, where the material of different density would be expected, we found many cysts with a desiccated appearance (Fig. S2B, pellet 2). Thus, room humidity will be important for researchers to monitor as they develop this model in their own facilities. Humidity may also play an important role in the seasonality that is seen with increases in human *E. histolytica* infections (41–43).

While the oral infection model presented herein does not recapitulate invasive disease associated with amebiasis caused by *E. histolytica*, we foresee its utility in investigating specific aspects of the *Entamoeba* life cycle that could not be achieved *in vivo* previously. It is important to note that only a small subset of cases involving *E. histolytica* infection become invasive, while the majority of *E. histolytica* infections remain confined to the large intestine and are either asymptomatic or mild to moderate in disease severity. Our model will open new avenues to study biological processes of *Entamoeba*, such as oral infection and excystation, persistence within the host, interactions with the immune system and the resident gut microbiome, and finally cyst formation and viability. The abundance of cysts produced in this model will also be useful for improving detection methods. Lastly, we have confidence that with further studies, by our and other groups, the establishment of a robust culturing protocol is attainable to study parasite-microbiome interactions *in vitro*. We are excited to present these results, which allow for a myriad of new research avenues focusing on parasite physiology, host-parasite interactions, and transmission.

MATERIALS AND METHODS

All mice were treated according to the guidelines established by the Institutional Animal Care and Use Committee (IACUC) of the University of Wisconsin School of Medicine and Public Health (protocol

number M005217). The institution adheres to the regulations and guidelines set by the National Research Council.

Screen for colonized mice. Fecal samples were collected from various institutions within the continental United States (Table S2), as well as our own vivarium facility. Genomic DNA (gDNA) was isolated following previously published protocols with the following modifications (44, 45): briefly, whole feces (~0.10 g) were placed in solvent-resistant screw-cap tubes containing 0.1 mm zirconia/silica beads (BioSpec Products 11079101z) and 1 large stainless steel bead (BioSpec Products 11079132ss) suspended in 20% SDS buffer (200 mM Tris·HCl, pH 8.0/200 mM NaCl/20 mM EDTA) and UltraPure Phenol/Chloroform/Isoamyl alcohol, pH 7.9, 25:24:1 (Invitrogen 15593-049). Samples were bead beat on high for 3 min at room temperature, and gDNA was precipitated with 3 M sodium acetate and isopropanol overnight. gDNA was cleaned using DNA Clean & Concentrator 5 (Zymo Research D4004). For identification of *Entamoeba muris*, a set of pan-*Entamoeba* primers were designed by downloading full-length *Entamoeba* 18S rRNA sequences ($n = 63$, 25 *Entamoeba* species) from NCBI GenBank, aligning them in CLC Genomics Workbench v20.0.4 (Qiagen, Hilden, Germany), and identifying conserved regions to target forward and reverse primers (Forward: 5′-AGATA CCGTCGTAGTCCT-3′ and Reverse: 5′-ACGACTTCTCCTTCCTCTAA-3′) which together amplify a 1 kb product (Fig. S1, reaction 1). A total of 500 ng per PCR were the genetic template for reaction 1, while for some samples a 2-step, nested PCR, was performed using 5 μL of reaction 1 as genetic template, using the same primer set and thermocycler conditions.

Cyst purification. Cyst counts: Fecal samples were processed used sucrose gradients as previously described with some modifications (46). Briefly, fecal samples (0.25 to 5 g) were ground to a fine powder using a mortar and pestle then shortly homogenized with Nanopure water for 15 min using a Mini Rotator (Glas-Col) at 60 rpm. The resulting solution was filtered through four-ply cotton gauze, and samples were pelleted for 10 min at 2500 $\times$ *g*. The resulting pellet layered on top of 1.5 M sucrose solution. The mid-layer was washed with Nanopure H_2O and pelleted again at same speed. Isolated, unfixed cysts were used as the input for oral infection.

Immunofluorescence assays. Fresh fecal sample was used to isolate cysts as described above then fixed in 10% formalin, washed twice, and resuspended. Isolated cysts were blocked for 5 min in 3% normal goat serum at room temperature with rotation. After washing, primary antibody 1A4 (22) was added at 1:1000 dilution (2.9 μg/mL concentration) and incubated for 2 h with rotation. As the secondary antibody, we utilized a goat anti-mouse IgG conjugated to Alexa Fluor 594 (Thermo Fischer Scientific) and incubated under the same conditions overnight. A set of washes in between antibodies was conducted. Lastly, the samples were stained with 0.1% Calcofluor White Stain (Sigma-Aldrich) according to the manufacturer's instructions. To target nucleic acids, 0.025% Syto11 stain (Thermo Fisher Scientific) was used. Equal parts of sample and VECTASHIELD Mounting Media (Vector Laboratories) were utilized. Samples were visualized using an Axio Imager 2 microscope (Zeiss). Images were captured at 40$\times$ and $\times$100 magnification using the DAPI, DIC, GFP and TexRed channels.

Sanger sequencing and phylogenetic analysis. Approximately 1 kb products from the Pan-*Entamoeba* PCR above were gel purified using a Zymoclean Gel DNA Recovery kit (Zymo Research) and submitted to the UW-Madison Biotechnology Center for Sanger Sequencing using the amplification primers described above. Sanger reads were manually inspected and edited using Sequencher v10.1 (Gene Codes Corporation) and queried against NCBI GenBank using Megablast (47) and default parameters. Twenty-seven full-length 18S *Entamoeba* sequences were downloaded from NCBI GenBank and aligned, along with our consensus Sanger sequence, using CLC Genomics workbench v20.0.4 (final length 1033 positions). A phylogenetic tree was inferred from the alignment with PhyML v.1.8.1 (48) using the general time reversible (GTR) substitution model and 1000 bootstrapped data sets were used to estimate statistical confidences of clades. To quantify nucleotide-level distances within the clade containing our organism, a pairwise distance matrix was constructed with the 4 clade members in CLC Genomics Workbench v20.0.4.

Mouse infections. Characterization of *E. muris* oral infection: House-bred male and female Swiss Webster Outbred mice were used to characterize *Entamoeba muris* infection for biological replicate 1 (Fig. 2 and S3). Male and female Swiss Webster (CFW) Outbred mice, purchased from Charles River Laboratories, were used to characterize *Entamoeba muris* infection for biological replicates 2 to 4 (Fig. 2 and S3). Mice were 6 to 8 weeks of age at the time of oral challenge, individually caged, and provided enrichment for the duration of the experiments. All animals were gavage-fed either purified cysts (1×10^5) or 1$\times$ PBS as a control.

Paromomycin treatment: Male and female Swiss Webster (CFW) Outbred mice were purchased from Charles River Laboratories and used to test paromomycin efficacy against *Entamoeba muris* oral challenge. Mice were 8 to 15 weeks of age at the time of oral challenge, individually caged, and provided enrichment for the duration of the experiments. All animals were gavage-fed either purified cysts (7×10^4 due to limited input cyst amounts) or 1$\times$ PBS as a control. Treated mice were administered paromomycin sulfate (Research Products International) via drinking water (16 g/L) *ad libitum* for 7 days before switching to normal drinking water. Throughout the length of the experiments, mice consumed an average of 5 mL per day with no difference in water consumption between untreated and treated mice.

Localization: House-bred male and female Swiss Webster Outbred mice were infected and euthanized at 5 dpi. The entire murine intestine was isolated and placed in 1$\times$ PBS. The small intestine was divided into three sections. Starting from the stomach, the first third was determined to be the duodenum, the following section was labeled as the jejunum, and the most proximal to the cecum was labeled ileum. For the large intestine, the entire cecum pouch and colon were used as independent sections. Intestinal contents of each section and a generous scraping of the host epithelial layer were pelleted at 2500 $\times$ *g* at room temperature for 5 min. The pellet was then processed in the previously described gDNA extraction protocol.

Cyst quantification. Sucrose Gradient: Cysts were purified as described above. For sucrose gradients, ~0.25 g fecal sample were used to isolate cysts. The cysts were then counted using a hemocytometer, and fecal mass was used to normalize counts.

qPCR: For quantification of *Entamoeba muris* by qPCR detection, standard curves were generated with known concentrations of cysts (Fig. S5) and intercalated dye (Bio-Rad SsoAdvanced Universal SYBR green Supermix) using either a QuantStudio 7 Flex real-time PCR system or a StepOnePlus real-time PCR system (Applied Biosystems). Individual standard curves were generated specifically for each system. The standard curve for the QuantStudio 7 Flex PCR system ranged from 1,562 to 100,000 cysts (Fig. S4A) and was used to calculate cyst concentrations in all biological replicates of Fig. 2C and biological replicate 1 of Fig. 3B. The standard curve for the StepOnePlus PCR system ranged from 1,562 to 50,000 cysts (Fig. S4B) and was used to calculate cyst concentrations for biological replicate 2 of Fig. 3B. Primers were designed as described above for pan-*Entamoeba* PCR (Fig. S1), except here they were chosen to amplify a 200 bp product. The following primers were used: Forward: 5′-TCGAGATAAACGAGAGCGAAAG-3′ and Reverse: 5′-GTCAGGACTACGACGGTATCTA-3′. Fecal samples were collected, and ~0.10 g of whole feces were used as the starting material for gDNA isolation as described above. Per qPCR well, 100 ng of sample gDNA were loaded and analyzed. The total number of *E. muris* cysts present in each sample per nanogram of gDNA was calculated using the CT values of the experimental samples and the linear trendline equations of their respective standard curves.

Excystation assay. Assays were conducted as previously described for *Entamoeba invadens* (27). Briefly, isolated cysts were acid washed with 0.1 M HCl for 10 min, followed by a second wash with Nanopure water. Cysts were then inoculated into each excystation treatment condition at a final amount of 10,000 cysts per condition: Nanopure water, 1% bovine bile, 80 mM sodium bicarbonate, or a combination of both bovine bile and sodium bicarbonate. Samples were incubated for 24 h at room temperature, washed with Nanopure water, and fixed in 10% formalin. Fixed cysts were stained with 0.1% Calcofluor White. Cysts were mounted and visualized as described for immunofluorescence assays. A total of 50 cysts per biological replicate were scored per tested condition.

SUPPLEMENTAL MATERIAL

Supplemental material is available online only.

FIG S1, TIF file, 2.9 MB.

FIG S2, TIF file, 2.9 MB.

FIG S3, TIF file, 2.9 MB.

FIG S4, TIF file, 2.9 MB.

FIG S5, TIF file, 0.6 MB.

FIG S6, TIF file, 0.9 MB.

TABLE S1, DOCX file, 0.01 MB.

TABLE S2, DOCX file, 0.01 MB.

ACKNOWLEDGMENTS

We sincerely thank Upinder Singh and her lab for advice, and Jerry Cangelosi and his lab for the 1A4 anti-Jacob2 antibodies. We thank researchers from across the United States for providing mouse fecal samples. We also thank members of the Knoll lab (Nicole M. Davis, Billy J. Erazo Flores, Carlos J. Ramirez Flores, Katie M. Cataldo, and Jasmine N. Hughes) for assistance with experiments, software, as well as scientific advice. We thank Apoorva P. Maru and Sarah K. Wilson for their critical reading and editing of the manuscript.

This work was funded by the National Institutes of Health (R01-AI144016-01 [L.J.K.]; T32007215 [C.M.C.]; T32AI007414 [L.A.O.]), SciMed Graduate Research Scholars Fellowship from the University of Wisconsin-Madison (C.M.C. and M.Y.H.), E. Michael and Winona Foster Wisconsin Distinguished Graduate Fellowship from the Food Research Institute (C.M.C.), and the Robert H. and Carol L. Deibel Distinguished Graduate Fellowship in Probiotic Research from the Food Research Institute (M.Y.H.). Funding bodies had no role in the design of the study and collection, analysis, and interpretation of data, or in writing the manuscript.

REFERENCES

1. Kappus K, Lundgren R, Juranek D, Roberts J, Spencer HC. 1994. Intestinal parasitism in the United States: update on a continuing problem. American J Tropical Medicine and Hygiene 50:705–713. https://doi.org/10.4269/ajtmh.1994.50.705.
2. Singer R, Xu TH, Herrera LNS, Villar MJ, Faust KM, Hotez PJ, et al. 2020. Prevalence of intestinal parasites in a low-income Texas community. The American J Tropical Medicine and Hygiene 102(6):1386–1395. https://doi.org/10.4269/ajtmh.19-0915.
3. Hotez PJ. 2014. Neglected parasitic infections and poverty in the United States. PLoS Negl Trop Dis 8(9):e3012. https://doi.org/10.1371/journal.pntd.0003012.
4. Liu L, Johnson HL, Cousens S, Perin J, Scott S, Lawn JE, Rudan I, Campbell H, Cibulskis R, Li M, Mathers C, Black RE, Child Health Epidemiology Reference Group of WHO and UNICEF. 2012. Global, regional, and national causes of child mortality: an updated systematic analysis for 2010 with time trends since 2000. Lancet 379:2151–2161. https://doi.org/10.1016/S0140-6736(12)60560-1.

5. Kotloff KL, Platts-Mills JA, Nasrin D, Roose A, Blackwelder WC, Levine MM. 2017. Global burden of diarrheal diseases among children in developing countries: incidence, etiology, and insights from new molecular diagnostic techniques. Vaccine 35:6783–6789. https://doi.org/10.1016/j.vaccine.2017.07.036.
6. Collaborators GDD. 2018. Estimates of the global, regional, and national morbidity, mortality, and aetiologies of diarrhoea in 195 countries: a systematic analysis for the Global Burden of Disease Study 2016. Lancet Infect Dis 18:1211–1228. https://doi.org/10.1016/S1473-3099(18)30362-1.
7. Shirley DT, Watanabe K, Moonah S. 2019. Significance of amebiasis: 10 reasons why neglecting amebiasis might come back to bite us in the gut. PLoS Negl Trop Dis 13:e0007744. https://doi.org/10.1371/journal.pntd.0007744.
8. Shirley D-AT, Farr L, Watanabe K, Moonah S. 2018. A Review of the Global Burden, New Diagnostics, and Current Therapeutics for Amebiasis. Open Forum Infect Dis 5:ofy161. https://doi.org/10.1093/ofid/ofy161.
9. Skappak C, Akierman S, Belga S, Novak K, Chadee K, Urbanski SJ, Church D, Beck PL. 2014. Invasive amoebiasis: a review of Entamoeba infections highlighted with case reports. Can J Gastroenterol Hepatol 28:355–359. https://doi.org/10.1155/2014/745130.
10. Lichtenstein A, Kondo AT, Visvesvara GS, Fernandez A, Paiva EF, Mauad T, Dolhnikoff M, Martins MA. 2005. Pulmonary amoebiasis presenting as superior vena cava syndrome. Thorax 60:350–352. https://doi.org/10.1136/thx.2004.021014.
11. Wuerz T, Kane JB, Boggild AK, Krajden S, Keystone JS, Fuksa M, Kain KC, Warren R, Kempston J, Anderson J. 2012. A review of amoebic liver abscess for clinicians in a nonendemic setting. Can J Gastroenterol 26:729–733. https://doi.org/10.1155/2012/852835.
12. Petri WA, Haque R. 2013. Entamoeba histolytica brain abscess. Handb Clin Neurol 114:147–152. https://doi.org/10.1016/B978-0-444-53490-3.00009-1.
13. Stanley SL. 2003. Amoebiasis. Lancet 361:1025–1034. https://doi.org/10.1016/S0140-6736(03)12830-9.
14. Haque R, Huston CD, Hughes M, Houpt E, Petri WA. 2003. Amebiasis. N Engl J Med 348:1565–1573. https://doi.org/10.1056/NEJMra022710.
15. Houpt ER, Glembocki DJ, Obrig TG, Moskaluk CA, Lockhart LA, Wright RL, Seaner RM, Keepers TR, Wilkins TD, Petri WA. 2002. The mouse model of amebic colitis reveals mouse strain susceptibility to infection and exacerbation of disease by CD4+ T cells. J Immunol 169:4496–4503. https://doi.org/10.4049/jimmunol.169.8.4496.
16. Wesel J, Shuman J, Bastuzel I, Dickerson J, Ingram-Smith C. 2021. Encystation of *Entamoeba histolytica* in Axenic Culture. Microorganisms 9:873. https://doi.org/10.3390/microorganisms9040873.
17. Aguilar-Díaz H, Díaz-Gallardo M, Laclette JP, Carrero JC. 2010. In vitro induction of entamoeba histolytica cyst-like structures from trophozoites. PLoS Negl Trop Dis 4:e607. https://doi.org/10.1371/journal.pntd.0000607.
18. Barrón-González MP, Villarreal-Treviño L, Reséndez-Pérez D, Mata-Cárdenas BD, Morales-Vallarta MR. 2008. Entamoeba histolytica: cyst-like structures in vitro induction. Exp Parasitol 118:600–603. https://doi.org/10.1016/j.exppara.2007.11.002.
19. Debnath A, Rodriguez MA, Ankri S. 2019. Editorial: recent progresses in amebiasis. Front Cell Infect Microbiol 9:247. https://doi.org/10.3389/fcimb.2019.00247.
20. Mendoza Cavazos C, Knoll LJ. 2020. Entamoeba histolytica: five facts about modeling a complex human disease in rodents. PLoS Pathog 16:e1008950. https://doi.org/10.1371/journal.ppat.1008950.
21. Jyothi R, Foerster B, Hamelmann C, Shetty NP. 1993. Improved method for the concentration and purification of faecal cysts of Entamoeba histolytica for use as antigen. J Trop Med Hyg 96:249–250.
22. Spadafora LJ, Kearney MR, Siddique A, Ali IK, Gilchrist CA, Arju T, Hoffstrom B, Nguyen FK, Petri WA, Haque R, Cangelosi GA. 2016. Species-specific immunodetection of an entamoeba histolytica cyst wall protein. PLoS Negl Trop Dis 10:e0004697. https://doi.org/10.1371/journal.pntd.0004697.
23. Ehrenkaufer GM, Suresh S, Solow-Cordero D, Singh U. 2018. High-throughput screening of entamoeba identifies compounds which target both life cycle stages and which are effective against metronidazole resistant parasites. Front Cell Infect Microbiol 8:276. https://doi.org/10.3389/fcimb.2018.00276.
24. Centers for Disease Control and Prevention. Amebiasis. 2013. https://www.cdc.gov/dpdx/amebiasis/tx.html.
25. Lee KC, Lu CC, Hu WH, Lin SE, Chen HH. 2015. Colonoscopic diagnosis of amebiasis: a case series and systematic review. Int J Colorectal Dis 30:31–41. https://doi.org/10.1007/s00384-014-2040-6.
26. Kantor M, Abrantes A, Estevez A, Schiller A, Torrent J, Gascon J, Hernandez R, Ochner C. 2018. Entamoeba histolytica: updates in clinical manifestation, pathogenesis, and vaccine development. Can J Gastroenterol Hepatol 2018:4601420.
27. Mitra BN, Pradel G, Frevert U, Eichinger D. 2010. Compounds of the upper gastrointestinal tract induce rapid and efficient excystation of Entamoeba invadens. Int J Parasitol 40:751–760. https://doi.org/10.1016/j.ijpara.2009.11.012.
28. Hamano S, Asgharpour A, Stroup SE, Wynn TA, Leiter EH, Houpt E. 2006. Resistance of C57BL/6 mice to amoebiasis is mediated by nonhemopoietic cells but requires hemopoietic IL-10 production. J Immunol 177:1208–1213. https://doi.org/10.4049/jimmunol.177.2.1208.
29. Chudnovskiy A, Mortha A, Kana V, Kennard A, Ramirez JD, Rahman A, Remark R, Mogno I, Ng R, Gnjatic S, Amir E-AD, Solovyov A, Greenbaum B, Clemente J, Faith J, Belkaid Y, Grigg ME, Merad M. 2016. Host-protozoan interactions protect from mucosal infections through activation of the inflammasome. Cell 167:444–456.e14. https://doi.org/10.1016/j.cell.2016.08.076.
30. Ghosh SK, Van Dellen KL, Chatterjee A, Dey T, Haque R, Robbins PW, Samuelson J. 2010. The Jacob2 lectin of the Entamoeba histolytica cyst wall binds chitin and is polymorphic. PLoS Negl Trop Dis 4:e750. https://doi.org/10.1371/journal.pntd.0000750.
31. Pittman KJ, Cervantes PW, Knoll LJ. 2016. Z-DNA binding protein mediates host control of Toxoplasma gondii infection. Infect Immun 84:3063–3070. https://doi.org/10.1128/IAI.00511-16.
32. Cervantes PW, Di Genova BM, Erazo FB, Knoll LJ. 2021. RIPK3 facilitates host resistance to oral *Toxoplasma gondii* infection. Infect Immun 89:e00021-21. https://doi.org/10.1128/IAI.00021-21.
33. Sunagar R, Kumar S, Namjoshi P, Rosa SJ, Hazlett KRO, Gosselin EJ. 2018. Evaluation of an outbred mouse model for Francisella tularensis vaccine development and testing. PLoS One 13:e0207587. https://doi.org/10.1371/journal.pone.0207587.
34. Watanabe H, Numata K, Ito T, Takagi K, Matsukawa A. 2004. Innate immune response in Th1- and Th2-dominant mouse strains. Shock 22:460–466. https://doi.org/10.1097/01.shk.0000142249.08135.e9.
35. Ferreira BL, Ferreira ÉR, de Brito MV, Salu BR, Oliva MLV, Mortara RA, Orikaza CM. 2018. BALB/c and C57BL/6 Mice cytokine responses to. Front Microbiol 9:553. https://doi.org/10.3389/fmicb.2018.00553.
36. Hartmann W, Blankenhaus B, Brunn ML, Meiners J, Breloer M. 2021. Elucidating different pattern of immunoregulation in BALB/c and C57BL/6 mice and their F1 progeny. Sci Rep 11:1536. https://doi.org/10.1038/s41598-020-79477-7.
37. Denic S, Nicholls MG. 2007. Genetic benefits of consanguinity through selection of genotypes protective against malaria. Hum Biol 79:145–158. https://doi.org/10.1353/hub.2007.0030.
38. Benton CH, Delahay RJ, Smith FAP, Robertson A, McDonald RA, Young AJ, Burke TA, Hodgson D. 2018. Inbreeding intensifies sex- and age-dependent disease in a wild mammal. J Anim Ecol 87:1500–1511. https://doi.org/10.1111/1365-2656.12878.
39. Churchill GA, Airey DC, Allayee H, Angel JM, Attie AD, Beatty J, et al. 2004. The Collaborative Cross, a community resource for the genetic analysis of complex traits. Nature Genetics 36:1133–1137. https://doi.org/10.1155/2014/210385.
40. Alum A, Absar IM, Asaad H, Rubino JR, Ijaz MK. 2014. Impact of environmental conditions on the survival of cryptosporidium and giardia on environmental surfaces. Interdisciplinary perspectives on Infectious Diseases 2014.
41. Pawestri AR, Thima K, Leetachewa S, Maneekan P, Deesitthivech O, Pinna C, Yingtaweesak T, Moonsom S. 2021. Seasonal prevalence, risk factors, and One Health intervention for prevention of intestinal parasitic infection in underprivileged communities on the Thai-Myanmar border. Int J Infect Dis 105:152–160. https://doi.org/10.1016/j.ijid.2021.02.015.
42. Jaran AS. 2017. Prevalence and seasonal variation of human intestinal parasites in patients attending hospital with abdominal symptoms in northern Jordan. East Mediterr Health J 22:756–760. https://doi.org/10.26719/2016.22.10.756.
43. Chowdhury FR, Ibrahim QSU, Bari MS, Alam MMJ, Dunachie SJ, Rodriguez-Morales AJ, Patwary MI. 2020. Correction: the association between temperature, rainfall and humidity with common climate-sensitive infectious diseases in Bangladesh. PLoS One 15:e0232285. https://doi.org/10.1371/journal.pone.0232285.
44. Turnbaugh PJ, Hamady M, Yatsunenko T, Cantarel BL, Duncan A, Ley RE, Sogin ML, Jones WJ, Roe BA, Affourtit JP, Egholm M, Henrissat B, Heath AC, Knight R, Gordon JI. 2009. A core gut microbiome in obese and lean twins. Nature 457:480–484. https://doi.org/10.1038/nature07540.
45. McNulty NP, Yatsunenko T, Hsiao A, Faith JJ, Muegge BD, Goodman AL, et al. 2011. The impact of a consortium of fermented milk strains on the gut microbiome of gnotobiotic mice and monozygotic twins. Sci Transl Med 3:106ra.

46. Walderich B, Müller L, Bracha R, Knobloch J, Burchard GD. 1997. A new method for isolation and differentiation of native Entamoeba histolytica and E. dispar cysts from fecal samples. Parasitol Res 83:719–721. https://doi.org/10.1007/s004360050326.
47. Morgulis A, Coulouris G, Raytselis Y, Madden TL, Agarwala R, Schäffer AA. 2008. Database indexing for production MegaBLAST searches. Bioinformatics 24:1757–1764. https://doi.org/10.1093/bioinformatics/btn322.
48. Guindon S, Dufayard JF, Lefort V, Anisimova M, Hordijk W, Gascuel O. 2010. New algorithms and methods to estimate maximum-likelihood phylogenies: assessing the performance of PhyML 3.0. Syst Biol 59:307–321. https://doi.org/10.1093/sysbio/syq010.